JOURNAL OF MATERIALS SCIENCE 26 (1991) 1205–1210

Carburation of an $Ni_{70}Cr_{30}$ substrate by laser solid-state diffusion

L. MARTIN, C. RENARD, C. BOURDA, T. PUIG
Etablissement Technique Central de l'Armement, 16 bis Avenue Prieur de la Côte d'Or, 94114 Arcueil, France

Laser surface treatments provide interesting solutions to the problem of accelerated wear of materials. Some results are presented for chromium carbide-rich surface alloys after laser-beam solid-state treatment of an $Ni_{70}Cr_{30}$ carbon-precoated substrate. The wear results are satisfactory with respect to pure $Ni_{70}Cr_{30}$ substrate, but are below those obtained by superficial melting of a graphitized $Ni_{70}Cr_{30}$ substrate.

1. Introduction

Laser treatments enable modification of the characteristics of a material, particularly by the formation of a superficial alloy. Moreover, structures reinforced with chromium carbides are of interest for the improvement of wear resistance and mechanical strength [1–6]. A better tribological behaviour of Nimonic 80A superalloy [7] (wear rate divided by 100) has already been obtained by injection of chromium carbide powders in the laser beam. The superficial fusion by a laser of an initially graphitized $Ni_{70}Cr_{30}$ substrate gives submicronic eutectic cellular structures (chromium carbide-γ solid solution) [8].

The purpose of the present study was to characterize the structures obtained by laser solid-state treatment of a graphitized $Ni_{70}Cr_{30}$ substrate and to understand the elementary processes which govern this type of treatment.

2. Experimental conditions

For all experiments the samples (width 10 mm, length 80 mm, thickness 10 mm) of $Ni_{70}Cr_{30}$ were irradiated by a Spectra Physics (CO_2, 5 kW, multimode) laser. To increase the thickness of the carbide-rich layer, several passes were necessary. A fresh carbon deposit (20 to 30 μm thick) was sprayed before each new pass. After the last treatment the carbon layer was removed by immersion in an ultrasonic water bath.

To avoid laser beam heterogeneity an homogenizer (kaleidoscope, 10 × 10 × 200 mm) was used. The uniform spot size (10 mm × 10 mm), treatment speed (5 mm sec^{-1}) and power of the laser beam (2.7 kW) were maintained constant. For all experiments, four thermocouples (nickel chromium/nickel aluminium) and two optical pyrometers (Maurer, 1 μm, and ATL 1000, 3 to 5 μm) were used (Fig. 1).

Before scanning electron microscopic (SEM) ana-

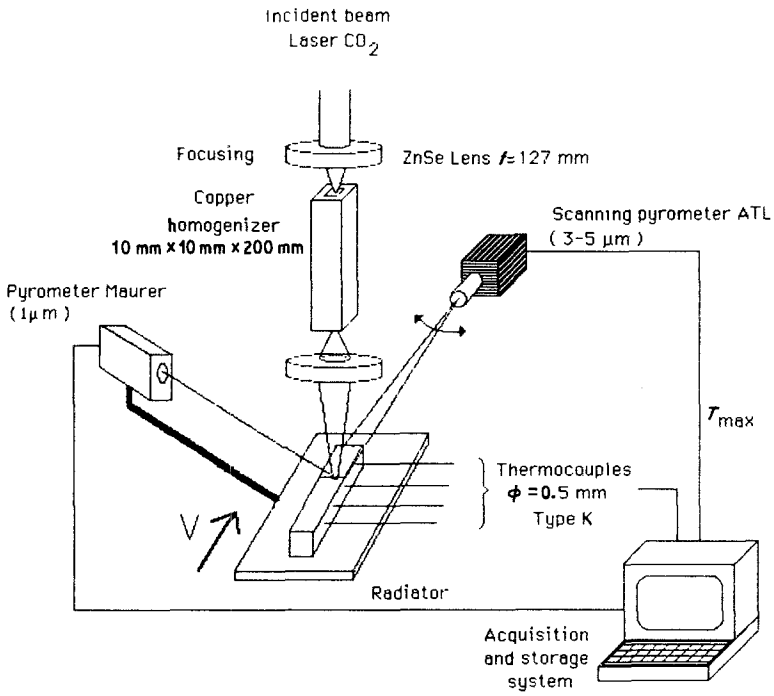

Figure 1 Optical apparatus.

0022–2461/91 $03.00 + .12

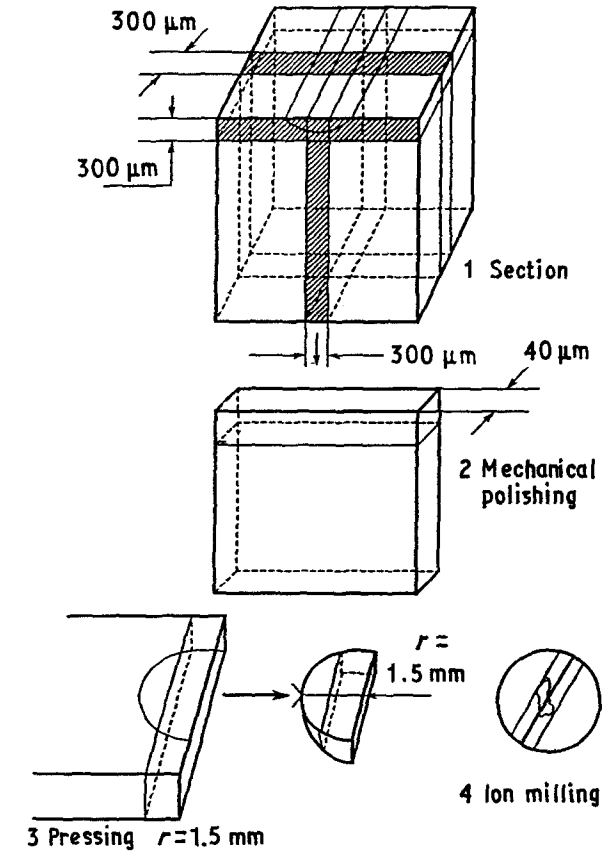

Figure 2 Thin foil preparation.

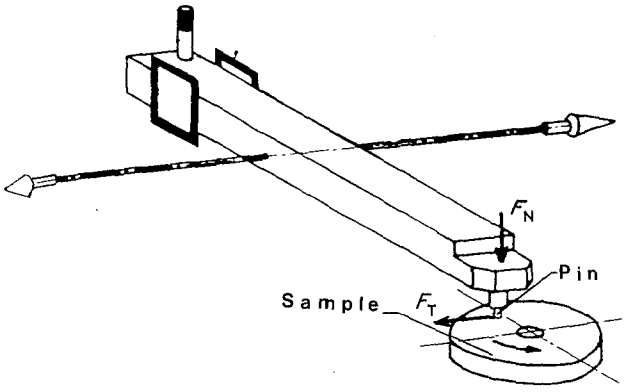

Figure 3 Pin-on-disc tribometer.

lysis, structures were revealed by Aqua Regia reagent (nitric acid (1.33) 25 ml, hydrochloric acid (1.19) 75 ml). Transmission electron microscopic (TEM) analysis was performed using Jeol 1200 EX and Jeol 2000 EX microscopes.

Foil preparation is described in Fig. 2.

The carbon concentration profiles were obtained using a nuclear microprobe (< 10 µm). The nuclear reaction used was ^{12}C (d, p)^{13}C (energy of deuterons = 1.4 MeV).

The pin-on-disc tribological test apparatus is shown in Fig. 3.

3. Results

3.1. Microstructural characterization

Precipitation is observed in the matrix and at grain boundaries: a volumic and intergranular diffusion is thus pin-pointed (Fig. 4). TEM analysis (micro-diffraction) allows the nature of the precipitated phases to be determined.

In all cases, the sequence of the appearance of the phases is the same from the top to the bottom of the tracks:

Cr_3C_2 (orthorhombic, $a = 1.146$ nm, $b = 0.552$ nm, $c = 0.282$ nm)

M_7C_3 (hexagonal, $a = 1.399$ nm, $c = 0.452$ nm; Fig. 5)

$M_{23}C_6$ (face centred cubic, $a = 1.074$ nm; Fig. 6).

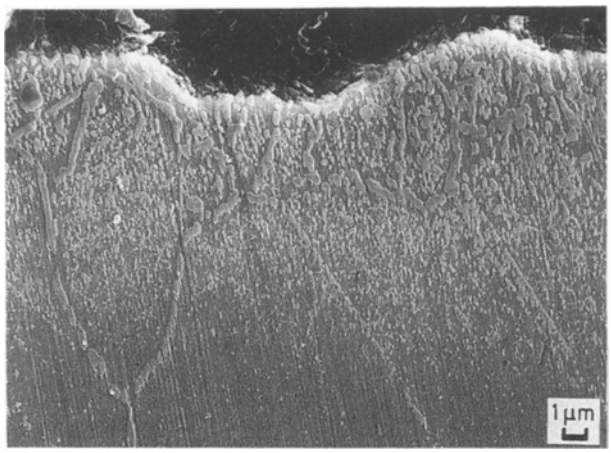

Figure 4 SEM analysis. Precipitation of carbides in the matrix and at grain boundaries.

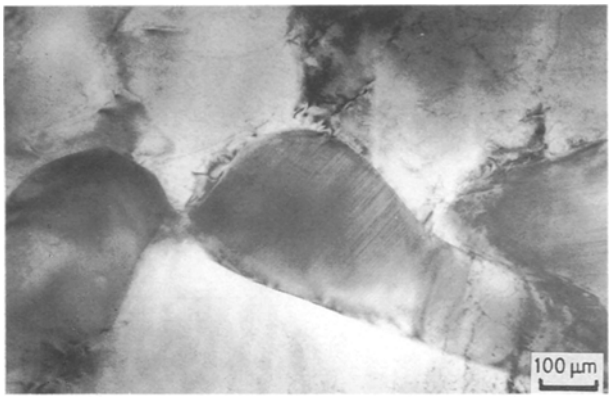

Figure 5 TEM analysis. Precipitation of M_7C_3 carbides at grain boundaries.

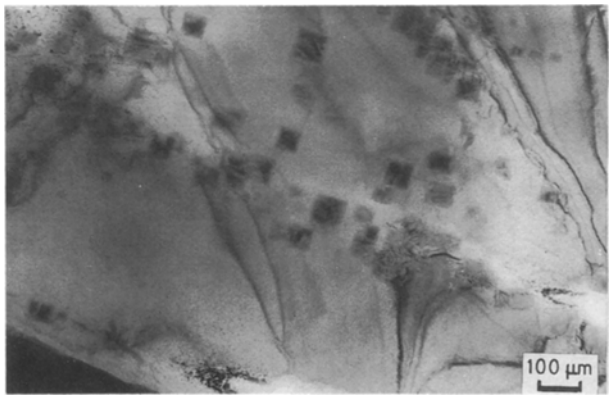

Figure 6 TEM analysis. Precipitation of $M_{23}C_6$ carbides in the matrix.

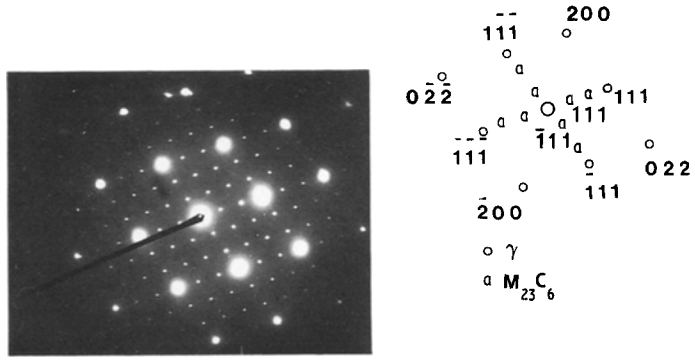

Figure 7 Diffraction pattern. Epitaxy between $M_{23}C_6$ and the γ-matrix.

An orientation relationship exists between the carbide $M_{23}C_6$ and the γ-matrix. The phases are in a simple cube–cube configuration $((0\,0\,1)_{M_{23}C_6} \| (0\,0\,1)_\gamma$ and $[1\,0\,0]_{M_{23}C_6} \| [1\,0\,0]_\gamma$; Fig. 7). Such orientation relationships have been reported by Double and Zambelli [9] in the study of directionally solidified (Co, Ni)–$Cr_{23}C_6$ eutectic alloy.

3.2. Analysis of the elements carbon, chromium and nickel

The analysis was carried out from the surface (Fig. 8) in the middle part of the tracks, using a nuclear microprobe (Fig. 9). It was noticed that the ratio of the number of X-photons emitted by the nickel atoms to the chromium ones does not vary very much with depth (Fig. 9, right-hand ordinate). Assuming that this ratio is a constant (%Ni/%Cr mass = 70/30) it is possible to determine the atomic concentration profiles in carbon (Fig. 9, left-hand ordinate).

Generally, it may be observed that the carbon concentration decreases continually from the surface to the bottom of the treated zone.

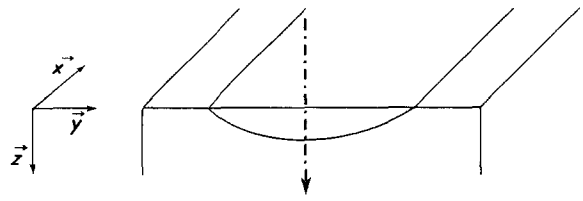

Figure 8 Microprobe analysis following the *z*-axis.

3.3. Pin-on-disc tribological tests

Two steps are observed during the tribological tests (Fig. 10):

(1) slight wear of the carburized matrix;

(2) serious wear of the underlying substrate.

Tests were made on several samples (untreated sample, 1, 2 and 5 laser passes). The time required for the pin to go through the carburized zone plotted against the number of treatments is shown in Fig. 11. With five passes, the time is 600 min (wear speed 10.3 nm sec^{-1}).

These results are below those obtained by liquid state diffusion [10].

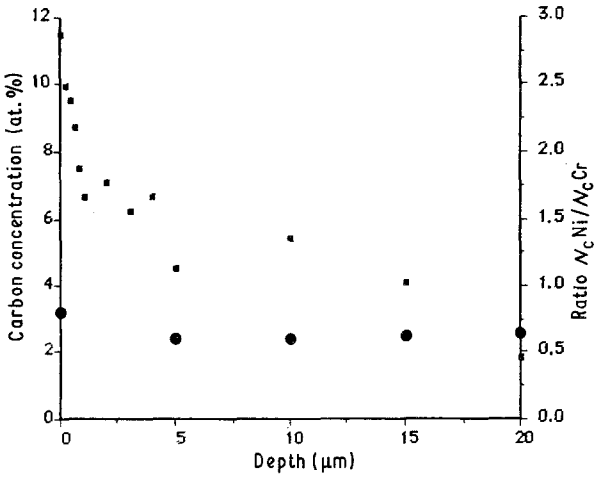

Figure 9 Profile of atomic concentration of carbon. Ratio of the number of X-rays emitted. (■) Analysis by nuclear microprobe; (●) N_cNi/N_cCr.

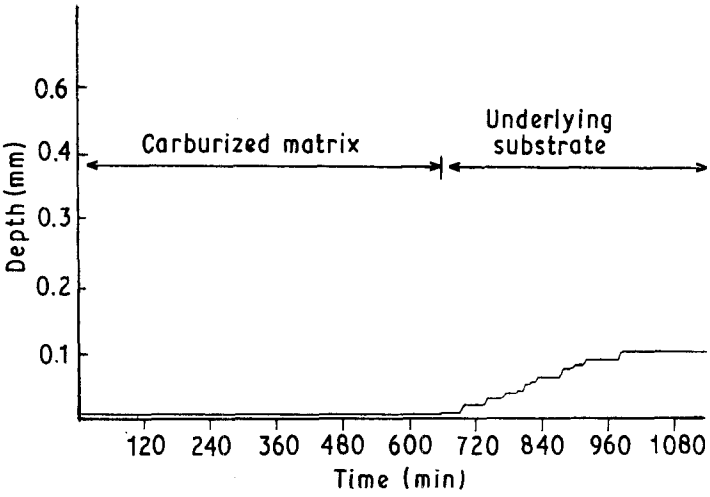

Figure 10 Tribological tests. Five passes.

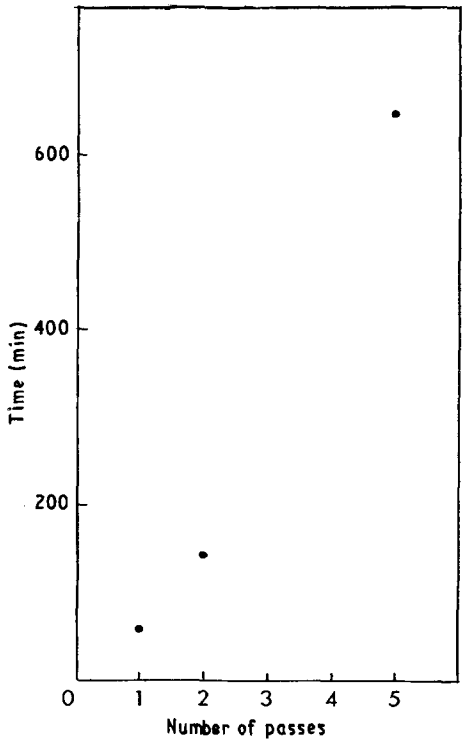

Figure 11 Life time of carburized zone plotted against the number of treatments.

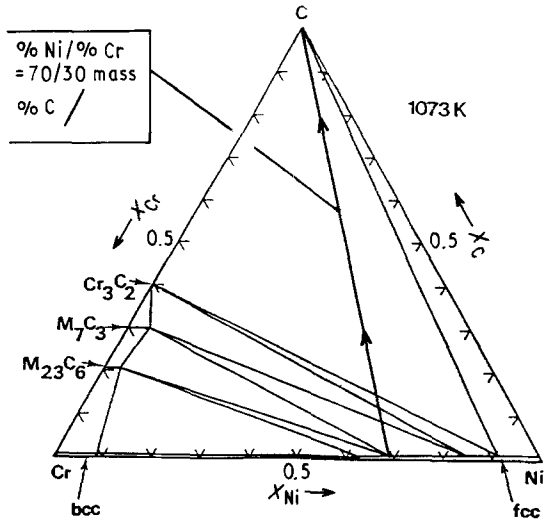

Figure 12 C–Cr–Ni ternary diagram at 1073 K.

4. Discussion

4.1. Ternary phase diagram at 1073 K

To correlate the concentration profiles (see Section 3.2) to the structural analysis, the different phase equilibria (%Ni/%Cr mass = 70/30 and increasing % C) [10] were determined from the ternary phase diagram (Fig. 12). These different equilibria are summarized in Fig. 13. The succession of chromium carbides is: $M_{23}C_6$, M_7C_3, Cr_3C_2 for increasing carbon concentration. Although far from equilibrium during laser treatment, the succession of chromium carbides is the same as that given by the diagram at equilibrium. This result has also been found in the case of liquid-state diffusion [10].

4.2. Model of thermal transfers

It was assumed that the thermal evolution in the material during laser irradiation could be described by the following one-dimensional heat diffusion equation [11].

$$\rho c(\partial T/\partial t) = \alpha(T)I(x,t) + \partial/\partial x[k(T)\partial T/\partial x] \quad (1)$$

where $\rho(T)$ is the mass density ($kg\,m^{-3}$), $c(T)$ the specific heat capacity ($J\,kg^{-1}K^{-1}$), $\alpha(T)$ the optical absorption coefficient (m^{-1}), $k(T)$ the thermal conductivity ($W\,m^{-1}K^{-1}$), $I(x,t)$ the power density ($W\,m^{-2}$), T the temperature (K), t the time (sec), and x the depth (m). Because α, ρ and k are generally temperature dependent, numerical methods were required to solve Equation 1. In the present work the irradiated region was divided into n layers of equal thickness, Δx. A relation between the temperature of the layer i at time $t + \Delta t$ and the temperature at time t can also be obtained.

$$T_i = T_i^0 + (\Delta Q_i^{abs} + \Delta Q_i^{dif})/(\rho c \Delta z) \quad (2)$$

where T_i is the temperature of layer i at time $t + \Delta t$, T_i^0 the temperature of the layer i at time t, $\Delta Q_i^{abs} = (I_i - I_{i+1})\Delta T$, $I_i = (1 - R)I_{i-1}\exp - \alpha i \Delta z$ is the power density absorbed at depth $i\Delta z$, R the reflection coefficient, and $\Delta Q_i^{dif} = 2k/\Delta z(T_{i-1}^0 + T_{i+1}^0 - 2T_i)\Delta t$. The different parameters used are summarized in Table I.

TABLE I Parameters used

Initial temperature	300 K
Mass density	$7800\,kg\,m^{-3}$
Specific heat capacity	$400\,J\,kg^{-1}\,K^{-1}$
Optical absorption coefficient	$24.49\,\mu m^{-1}$
Thermal conductivity	$10\,W\,m^{-1}K^{-1}$
Reflection coefficient	0.25
Perfect gas constant	$2\,cal\,mol^{-1}$
Frequency factor	$2.49 \times 10^{-4}\,m^2\,sec^{-1}$
Activation energy	$40\,000\,cal\,mol^{-1}K^{-1}$

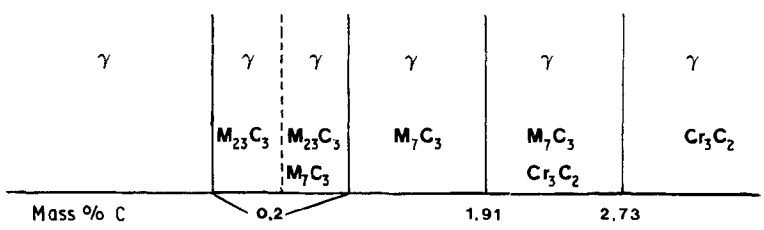

Figure 13 Succession of chromium carbides for increasing carbon concentration.

The present results were compared with those calculated with a two-dimensional model by finite elements (THERM 2D) [12]. The correlation between both models is very satisfactory.

4.3. Model of the carbon distribution during beam interaction

The redistribution in carbon was calculated using a one-dimensional model with an explicit resolution diagram. The diffusion of the carbon volume within the affected bulk is considered to be unidirectional. The carbon diffusion coefficient depends on the temperature calculated using a thermal model (see Equations 1 and 2) [13]

$$D = D_0 \exp - Q/RT \quad (3)$$

where D is the carbon in nickel diffusion coefficient, D_0 the frequency factor ($m^2 sec^{-1}$), Q the activation energy ($cal\,mol^{-1}K^{-1}$), and R the perfect gas constant. It is possible, assuming that the concentration of each layer, i, is a constant between t and $t + \Delta t$, to determine a spatial and temporal relation between the carbon concentrations

$$C_i = C_i^0 + D\Delta t/\Delta z^2(C_{i+1}^0 + C_{i-1}^0 - 2C_i^0) \quad (4)$$

where C_i is the atomic concentration of carbon of layer i at time $t + \Delta t$, and C_i^0 is the atomic concentration of carbon of layer i at time t. The results of the calculation (see Table I) are shown in Fig. 14. The differences between calculated and measured values can be explained as follows.

1. The diffusion model is only volumetric and does not take into account the diffusion short circuits (grains boundaries, dislocations, carbides).
2. The variation of the frequency factor (D_0) with carbon concentration is neglected.

From the calculated profile, it is possible to determine the depth of the initial deposit concerned, by the diffusion at each pass. This depth (0.5 μm) is less than the initial deposit obtained by spraying (20 to 30 μm).

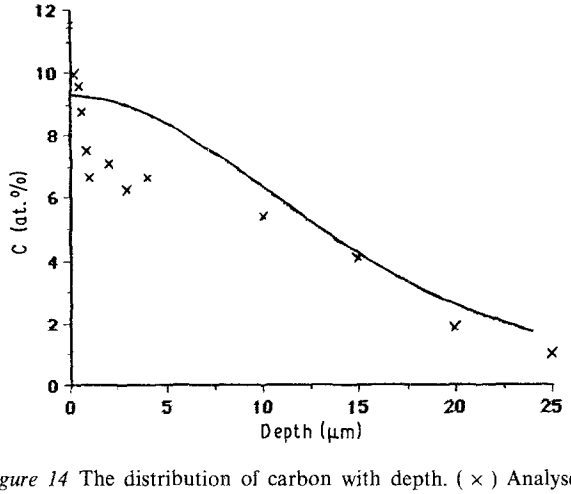

Figure 14 The distribution of carbon with depth. (×) Analysed profile; (——) calculated profile.

The main reason for this is probably the fact that the deposit is not bulky, but made of an aggregate of powders with an organic liant.

4.4. Tribological tests

Tribological results obtained after solid state diffusion are below those observed in the case of liquid-state diffusion [10]. Two explanations can be given.

1. The carbide volume fraction is more important in the case of liquid-state diffusion (carbon diffusion depth 90 μm).
2. Structures obtained after liquid-state diffusion are eutectic and submicronic. Tribological behaviour is much better.

5. Conclusions

1. Chromium carbide formation can be obtained at a depth of about 10 μm for treatment duration of about 10 sec.
2. Although far from equilibrium (laser treatment), a correlation exists between the structures obtained and those given by the isothermal section of the corresponding ternary phase diagram, C–Cr–Ni.
3. A one-dimensional model can be used to describe qualitatively the carbon diffusion.
4. The low carbides volume fraction is due to the poor initial carbon deposit. Tribological results fall below those obtained by liquid-state diffusion; these results could be adequate for wear applications which were not too hard.

Acknowledgements

The authors thank Messrs Kechemair, Bataille, Ricaud and Sabatier for their assistance with experiment instrumentation and in the use of THERM 2D, Mrs Mosbah and Messrs Trocellier and Gosset for their knowledge of microprobe analysis, and Messrs Fachinetti, Dubois and Duverneix for their assistance.

References

1. J. D. REARDON, R. MIGNOGNA and F. N. LONGO, *Thin Solid Film* **85** (1981) 345.
2. G. Y. LAI, *ibid.* **53** (1978) 343.
3. *Idem, ibid.* **64** (1979) 271.
4. F. D. LEMKEY and E. R. THOMPSON, US Pat. 3 564 940 (1966).
5. E. R. THOMPSON and F. D. LEMKEY, *Met. Trans.* **1** (1970) 2799.
6. *Idem*, in "Directionally solidified eutectics superalloys. Composites Materials", Vol. 4, edited by L. J. Broutman and R. H. Krock (Academic Press, London, 1974) p. 102.
7. T. PUIG, J. L. DEREP, J. L. FACHINETTI and G. COQUERELLE, *Mater. Sci. Engng* **88** (1987) 151–156.

8. T. PUIG, J. L. DEREP, G. COQUERELLE and M. CONDAT, "Formation de carbures de chrome sur un alliage NiCr", Annales de chimie, Science des Matériaux, Vol. 13 (Masson, Paris, 1988) pp. 317–25.
9. D. D. DOUBLE and G. ZAMBELLI, *J. Mater. Sci.* **13** (1978) 534.
10. T. PUIG, Thèse Université Paris-Sud, Orsay, France (1989).
11. C. K. ONG, H. S. TAN and E. H. SIN, *Mater. Sci. Engng* **79** (1986) 79.
12. D. KECHEMAIR, Thèse Université Paris VI, Orsay, France (1989).
13. Y. ADDA and J. PHILIBERT, "La diffusion dans les solides", Vol. II (Bibliothèque des Sciences et Techniques Nucléaires, Saclay, 1966) p. 1186.

Received 10 August 1989
and accepted 9 January 1990